TECHNICAL PAPER

Model-free adaptive variable impedance control of gait rehabilitation exoskeleton

Mehdi Bakhtiari[1] · Mohammad Reza Haghjoo[1] · Mostafa Taghizadeh[1]

Abstract

This paper addresses the challenges of control and human–robot interaction for lower-limb gait rehabilitation exoskeletons. To enhance the robustness of the control against unknown but bounded uncertainties, we propose a model-free adaptive sliding mode control strategy enhanced by a variable impedance approach. The adaptation law prevents the overestimation of control gain in the presence of uncertainty and ensures the sliding condition to mitigate the effects of unknown uncertainties. The variable impedance approach also allows the impedance of the entire system to adapt dynamically over the gait cycle and maintain the accuracy of the robot in tracking desired joint trajectories. We provide a detailed stability proof using Lyapunov theory and demonstrate the finite-time convergence of the defined sliding surface. The proposed strategy does not require knowledge of model parameters, resulting in reduced computational complexity. A lower extremity rehabilitation exoskeleton model was utilized as an illustrative example. To demonstrate the effectiveness of the proposed approach, we conducted several simulations using a lower-limb rehabilitation exoskeleton model. Comparative evaluations were performed against conventional control methods such as the conventional sliding mode and computed torque controllers. The results indicate the effective performance of the proposed controller in the presence of impedance, in reducing the detrimental effects of interaction forces and model uncertainty, as well as accurately tracking the desired gait trajectories.

1 Introduction

Lower-limb rehabilitation plays a crucial role in improving mobility and autonomy for individuals affected by stroke and other conditions that cause lower-limb impairments [1–3]. Scientific studies have proven the efficacy of repetitive and intensive rehabilitation training in restoring ambulatory function. Traditionally, lower-limb rehabilitation relies on manual assistance from two or three therapists to facilitate

---

Technical Editor: Rogério Sales Gonçalves.

✉ Mohammad Reza Haghjoo
  m_haghjoo@sbu.ac.ir

  Mehdi Bakhtiari
  m_bakhtiari@sbu.ac.ir

  Mostafa Taghizadeh
  mo_taghizadeh@sbu.ac.ir

[1] Faculty of Mechanical and Energy Engineering, Shahid Beheshti University, Tehran, Iran

leg mobilization and ensure postural stability. However, the increasing labor burden and healthcare costs have led to a demand for the development of robotized systems as an alternative to therapists for implementing rehabilitation interventions [4, 5].

Robotic rehabilitation has gained significant attention in recent years due to its effectiveness in treating motor impairments. Among the various robots used in rehabilitation, exoskeletons [6] have emerged as an important category since the 1960s in America, Japan, and Europe [7]. The Lokomat is a well-known example of such robotic systems [8, 9]. These wearable robots are designed with joints aligned coaxially with the patient's joints, allowing the patient's body to replicate predetermined therapeutic movements [10]. Precise control of joint positions and effective management of interactive forces between the robot and the patient are essential factors in the control of exoskeleton robots [11]. The design of an appropriate controller directly influences the performance of the exoskeleton. The primary objective of this study is to develop an effective control methodology for

lower-limb rehabilitation systems that interact with patients and the environment.

Sliding mode control (SMC) is an effective control approach known for its ability to reject uncertainties, eliminate external disturbances, and be less sensitive to variations in the robot's parameters [12, 13]. However, it suffers from issues such as chattering and infinite-time convergence to the equilibrium point, which can be problematic for Euler–Lagrange systems [14]. To address these issues, several SMC-based methods have been proposed. Terminal sliding mode control (TSMC) guarantees finite-time convergence of the states to the equilibrium point [15–18]. High-order sliding mode control (HOSMC) promotes accuracy and eliminates chattering while retaining the robustness of conventional SMC [19]. Super-twisting-based second-order sliding mode control (SOSMC) has also shown promise in mitigating chattering and handling disturbances and uncertainties [20]. However, these control strategies rely on accurate model parameters or large amounts of data, which can be challenging to obtain in practical applications. To overcome this challenge, recent attention has been given to model-free adaptive and robust SMC strategies for uncertain and nonlinear robotic systems [21–23]. These strategies utilize an adaptation law to prevent the overestimation of control gain in the presence of uncertainty and ensure the sliding condition to mitigate the effects of unknown uncertainties.

In the case of joint injuries, it is essential for the robot to apply gentle force in the therapeutic direction to the affected joint [24–26]. Conversely, if the patient has joint mobility at other joints, the robot should enable the patient to exert their own force, promoting dynamic force interaction between the patient and the exoskeleton [27]. The Lokomat robot has used a combined control of force and position to enhance the patient's active participation in walking. This control structure consists of a closed-loop PD position controller and a force controller, with the two loops being switched between the swing and stand phases of walking separately [28]. However, the switching process is not explicitly known and may result in a nonphysiological gait pattern in the patient's walking.

The concept of impedance control is an effective approach used to uniformly reduce interaction forces of robots by incorporating a virtual mass, spring, and damper between the robot and a known environment [29]. Impedance and adaptive control approaches for lower-limb exoskeletons have been studied in various research projects, as seen in [30, 31]. Additionally, studies like [32–35] have proposed transparent or assist as-needed control methods for lower-limb exoskeletons, demonstrating advancements in able-bodied walking scenarios. These examples highlight the evolving landscape of control strategies in the field of rehabilitation robotics and emphasize the importance of exploring novel

methodologies to enhance the transparency of lower-limb exoskeletons.

In the realm of lower-limb rehabilitation exoskeletons, where uncertainties in dynamics and the need for adaptable interaction between users and robots are paramount, variable impedance control plays a vital role. Recent advancements have demonstrated the effectiveness of variable impedance control in enhancing adaptability and performance in various robotic systems facing complex interactions and uncertain environments [36–40]. However, the integration of variable impedance control with model-free adaptive sliding mode control strategies remains largely unexplored in the context of lower-limb rehabilitation exoskeletons.

The synergy between variable impedance control and adaptive sliding mode control holds immense potential for optimizing the rehabilitation process by offering a tailored and responsive interaction between the exoskeleton and the user. This integration combines the adaptability of variable impedance control with the stability and robustness of adaptive sliding mode control, offering a comprehensive framework to address the challenges unique to lower-limb rehabilitation scenarios.

In this research, the authors introduce a novel approach to address the adverse effects of interaction forces in lower-limb rehabilitation exoskeletons. Their method combines a model-free adaptive sliding mode control (SMC) framework with a variable impedance strategy. The adaptive law effectively prevents the overestimation of control gain under uncertain conditions, ensuring the system maintains the sliding condition to counter unknown uncertainties. Moreover, the variable impedance strategy enables the system's impedance to dynamically adjust throughout the gait cycle, enhancing the robot's precision in tracking desired joint trajectories. By aiming to sustain interactive forces close to zero at the patient-robot connection points while allowing system-wide impedance adaptation during gait, the approach prioritizes patient comfort and usability by avoiding disruptive and erratic forces.

The study includes a comprehensive stability analysis utilizing Lyapunov theory, demonstrating the finite-time convergence of the defined sliding surface. The adaptive sliding mode controller, designed based on Lyapunov theory, is instrumental in achieving these stability goals. The proposed control methodology is rigorously evaluated through simulations on a dynamic model using MATLAB SimScape, offering a comparative analysis against traditional control strategies.

The structure of the paper is as follows: Sect. 2 provides a detailed description of the lower-limb rehabilitation exoskeleton model and introduces its dynamic equations. It also presents the design of the proposed primary control algorithm, namely the model-free adaptive sliding mode

control. Additionally, the variable impedance strategy and the extended state observer are introduced in this section to enhance the primary controller. Section 3 presents the numerical simulation results and subsequent discussions. Finally, Sect. 4 concludes the paper and outline future research directions.

2 Materials and methods

Figure 1 illustrates the schematic of the rehabilitation robot being investigated. It is evident that the robot possesses the capability to engage with each leg of the patient through three active joints (hip abduction–adduction, hip extension-flexion, knee extension-flexion) and one passive joint (ankle dorsiflexion). The robot introduced in this study, as previously mentioned, is specifically designed with an exoskeleton-like architecture. It is worth noting that while many rehabilitation robots are typically designed to operate solely in the sagittal plane with only one degree of freedom for the hip, a more realistic representation can be achieved by considering two degrees of freedom for the hip joint, as reported in [41]. This approach allows for a more natural range of motion and better mimics the movements required for various activities. Therefore, in our research, we evaluate the exoskeleton under the most challenging conditions, even though it has been validated for more simplified structures. Notably, the alignment of the robot's joints with the patient's joints ensures congruity between their respective kinematics. The patient's ankle position relative to the pelvis is synchronized with the desired trajectory by the help of the

robot. Moreover, the ankle joint of the robot is facilitated by a torsion spring, enabling passive movement and preventing foot drop in the patient during rehabilitation [42]. The presented robot utilizes body weight support (BWS) and is capable of neutralizing the entire weight of the patient [34]. In Fig. 1, θ_i and L_i represent the angle and length of each link, respectively. Here, the angles θ_i, where i ranges from 1 to 3, are considered as the generalized coordinates of the system. Specifically, θ_1 corresponds to the hip abduction–adduction motion in the coronal plane, while θ_2 and θ_3 correspond to the hip and knee extension-flexion motions in the sagittal plane, respectively. In addition, m_i, C_{m_i}, and I_i respectively denote the mass, the center of mass position, and the moment of inertia of each link of the robot integrated with the corresponding leg part of the subject. To extract the dynamic relations governing the robot, the Lagrange method has been used in the form of Eq. (1)

$$\tau_i = \frac{d}{dt}\left(\frac{\partial K}{\partial \dot{\theta}_i}\right) - \frac{\partial K}{\partial \theta_i} + \frac{\partial U}{\partial \theta_i} \qquad (1)$$

Where K and U are the kinetic and potential energies of the robot and patient links, respectively. Also τ_i is the input torque applied to each joint of the robot. Briefly, the dynamic equations governing the robot are expressed in the form of Eq. (2).

$$\tau = M(\theta)\ddot{\theta} + C(\theta.\dot{\theta}) + G(\theta) + \tau_d \qquad (2)$$

Where $M(\theta)$ denotes the moment of inertia matrix, $C(\theta.\dot{\theta})$ is the matrix of centrifugal and Coriolis effects, and $G(q)$ is the vector of gravitational forces as
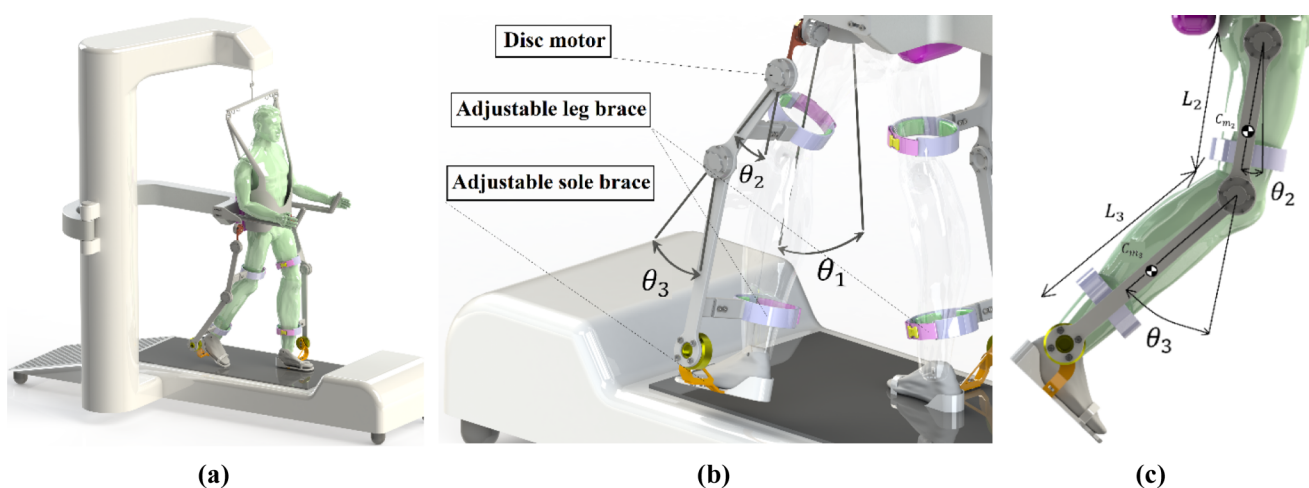
Fig.1 The schematic of **a** a typical lower body exoskeleton robot, **b** joint parameters definitions: θ_1 indicates the hip abduction–adduction angle in coronal plane; θ_2 and θ_3 indicate the hip and knee extension-flexion angles in the sagittal plane, respectively, **c** physical parameters definitions

$$M = \begin{bmatrix} I_2 + I_3 + m_2 C_{m_2}^2 + m_3 C_{m_3}^2 & m_3 L_2 C_{m_3} C(\theta_2) & m_3 L_3 C_{m_3} C(\theta_2 + \theta_3) \\ m_3 L_2 C_{m_3} C(\theta_2) & I_3 + m_3 C_{m_3}^2 & m_3 L_3 C_{m_3} C(\theta_3) \\ m_3 L_3 C_{m_3} C(\theta_2 + \theta_3) & m_3 L_3 C_{m_3} C(\theta_3) & I_3 \end{bmatrix} \tag{2-1}$$

$$C = \begin{bmatrix} -m_3 L_2 C_{m_3} S(\theta_2)\dot\theta_2 - m_3 L_3 C_{m_3} S(\theta_2 + \theta_3)(\dot\theta_2 + \dot\theta_3) & m_3 L_3 C_{m_3} S(\theta_2 + \theta_3)\theta_3 & -m_3 L_3 C_{m_3} S(\theta_2 + \theta_3) \\ m_3 L_2 C_{m_3} S(\theta_2)\dot\theta_1 & 0 & m_3 L_3 C_{m_3} S(\theta_3)\theta_3 \\ m_3 L_3 C_{m_3} S(\theta_2 + \theta_3)(\dot\theta_1 + \dot\theta_2) & -m_3 L_3 C_{m_3} S(\theta_3)\dot\theta_3 & 0 \end{bmatrix} \tag{2-2}$$

$$G = \begin{bmatrix} (m_2 C_{m_2} + m_3 C_{m_3}) g S(\theta_1) + m_3 L_2 C_{m_3} g S(\theta_1 + \theta_2) \\ m_3 L_2 C_{m_3} g S(\theta_1 + \theta_2) + m_3 L_3 C_{m_3} g S(\theta_1 + \theta_2 + \theta_3) \\ m_3 L_3 C_{m_3} g S(\theta_1 + \theta_2 + \theta_3) \end{bmatrix} \tag{2-3}$$

in witch $S(.)$ and $C(.)$ denote sin(.) and cos(.). Also τ_d represents the disturbance torques applied to the system that can disrupt its desired behavior [35, 43]. The above model of the robot can be rewritten in the following form as.

$$\ddot\theta = M^{-1}(\tau - C - G) - M^{-1}\tau_d \tag{3}$$

Assumption 1 The exogenous disturbances τ_d are bounded and $\|\tau_d\| \le \overline{\tau}_d < \infty$ in which $\overline{\tau}_d$ is an unknown variable.

Assumption 2: The matrices presenting the dynamic model of the system $M(\theta)$, $C(\theta.\theta)$, and $G(\theta)$ are bounded such that:

$$M(\theta) \le \overline{m}I \tag{4}$$

$$C\left\|C(\theta.\dot\theta) \le \overline{c}\dot\theta\right\| \tag{5}$$

$$\|G(\theta)\| \le \overline{g} \tag{6}$$

Where $\overline{m}$, $\overline{c}$ and $\overline{g}$ are upper bound positive constants and I denotes the identity matrix.

Property 1: For $\frac{1}{2}\dot M(\theta) - C(\theta.\dot\theta)$, the equality $x^T\left(\frac{1}{2}\dot M(\theta) - C(\theta.\dot\theta)\right)x = 0$ always holds for any x.

Property 2: The norms of the inertia matrix $M(\theta)$, $C(\theta)$, and $G(\theta)$ are bounded as considered in Assumption 2. This guarantees that the dynamic model of the system is bounded and can be effectively controlled.

2.1 Model-free adaptive sliding mode control

Consider the system dynamics, defined in Eq. (4), Eq. (5), and Eq. (6), with a combination of uncertainties and exogenous time-dependent bounded disturbances. Let us define the following error:

$$e = \theta - \theta_d \tag{7}$$

$$\dot e = \dot\theta - \dot\theta_d \tag{8}$$

where θ_d and $\dot\theta_d$ indicate the desired or reference joint angles and joint velocities, respectively. The basic sliding surface is defined as:

$$S = \dot e + \int_0^t \left(\lambda_1 \|e\|^p \frac{e}{\|e\|} + \lambda_2 \|\dot e\|^q \frac{\dot e}{\|\dot e\|}\right) d\tau \tag{9}$$

Then, its time derivative can be expressed as:

$$\dot S = \ddot\theta - \ddot\theta_d + \lambda_1 \|e\|^p \frac{e}{\|e\|} + \lambda_2 \|\dot e\|^q \frac{\dot e}{\|\dot e\|} \tag{10}$$

p and q are unit power terms that impact control adaptation on errors and error velocities, respectively, while λ is an adjustable parameter affecting adaptation rate in the presence of errors and uncertainties. Accordingly, the following time-varying sliding surface and adaptive model-free control law can be defined to compensate the negative effects of disturbances and uncertainties.

$$\dot S = \ddot\theta_d - M^{-1}\left(\tau_d + C\dot\theta + G - \tau\right) + \lambda_1 \|e\|^p \frac{e}{\|e\|} + \lambda_2 \|\dot e\|^q \frac{\dot e}{\|\dot e\|} \tag{11}$$

Multiplying by M yields:

$$M\dot S = \tau - CS + \Xi \tag{12}$$

$$\Xi = -\left[C\dot\theta + G + \tau_d - CS - M\ddot\theta_d - M\left(\lambda_1 \|e\|^p \frac{e}{\|e\|} + \lambda_2 \|\dot e\|^q \frac{\dot e}{\|\dot e\|}\right)\right] \tag{13}$$

According to property 1, $\|M\|$, $\|C\|$, and $\|G\|$ satisfy property 2. By defining $\Phi = \begin{bmatrix} e & \dot e \end{bmatrix}^T$, $\|e\| \le \|\Phi\| \& \|\dot e\| \le \|\Phi\|$, then:

$$\|\Xi\| \le \Omega_1 \|\Phi\|^0 + \Omega_2 \|\Phi\|^1 + \Omega_3 \|\Phi\|^2 \tag{14}$$

In Eq. (14), Ω_i are unknown terms and it should be noted that Assumption 1 does not impose a priori bounds on the lumped term. Accordingly, the following adaptive model-free sliding mode control law is defined as:

$$\tau_\eta = -\left[\Gamma S + \Lambda \text{sgn}(S)\right] \qquad (15)$$

$$\Lambda = \hat{\Omega}_1 \|\Phi\|^0 + \hat{\Omega}_2 \|\Phi\|^1 + \hat{\Omega}_3 \|\Phi\|^2 \qquad (16)$$

$$\dot{\hat{\Omega}}_i = \|S\| \cdot \|\Phi\|^{i-1} - \gamma_i \hat{\Omega}_i \qquad (17)$$

where Γ is a positive constant and τ_η represents the effecting control torque which can ensure the desired control performance. Note that $\hat{\Omega}_i(0) > 0$ and γ_i is a positive constant as $\gamma_i > 0$ for $i = 1,2,3$.

Theorem 1 Considering the dynamic model, globally uniformly ultimately bounded (GUUB) of the closed-loop system will be analyzed under the effect of the proposed control law in Eq. (15) where an ultimate bound ω on the sliding surface is

$\omega = \sqrt{\frac{\sum_{i=0}^{2} \gamma_i \kappa_i^2}{(\kappa - \eta)}}$ with $\triangleq 2 \min_i \left\{\Gamma, \frac{\gamma_i}{2}\right\} > 0$ and $0 < \eta < \kappa$.

Proof: To show the stability of the closed-loop system, the following Lyapunov function can be defined. For the sake of compactness, the time dependency is omitted in the subsequent derivation.

$$V = \frac{1}{2} S^T M S + \sum_{i=1}^{3} \frac{1}{2} \tilde{\Omega}_i^2 \qquad (18)$$

By taking the time derivative of Eq. (16):

Table 1 Physical parameters used in simulations

Physical parameters	Units	Normal values
L_2	*mm*	450
L_3	*mm*	375
m_2	*gr*	8780
m_3	*gr*	11580
C_{m_2}	*mm*	225
C_{m_3}	*mm*	185

Substituting Eq. (17) into Eq. (18), then:

$$\dot{V} \leq -\frac{\lambda(\Lambda)_{\min}}{n\|S\|^2 \sum_{i=1}^{3} \left[\gamma_i \hat{\Omega}_i \Omega_i - \gamma_i \hat{\Omega}_i^2\right]} \leq -\frac{\lambda(\Lambda)_{\min}}{n\|S\|^2 \sum_{i=1}^{3} \left[\frac{\gamma_i}{2} \tilde{\Omega}_i^2 - \frac{\gamma_i}{2} \Omega_i^2\right]} \qquad (21)$$

With $\lambda(\Lambda)_{\min}$ represents the minimum eigenvalue. Therefore, Eq. (19) can be rewritten as:
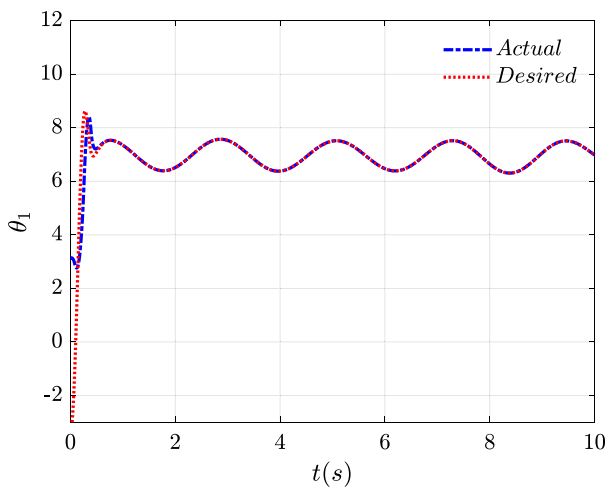
$$\dot{V} \leq -\frac{\lambda(\Lambda)_{\min}}{n\|S\|^2 \sum_{i=1}^{3} \left[\gamma_i \hat{\Omega}_i \Omega_i - \gamma_i \hat{\Omega}_i^2\right]} \leq -\frac{\overline{m}}{2} \|S\|^2 + \sum_{i=1}^{3} \frac{1}{2} \tilde{\Omega}_i^2 \qquad (22)$$

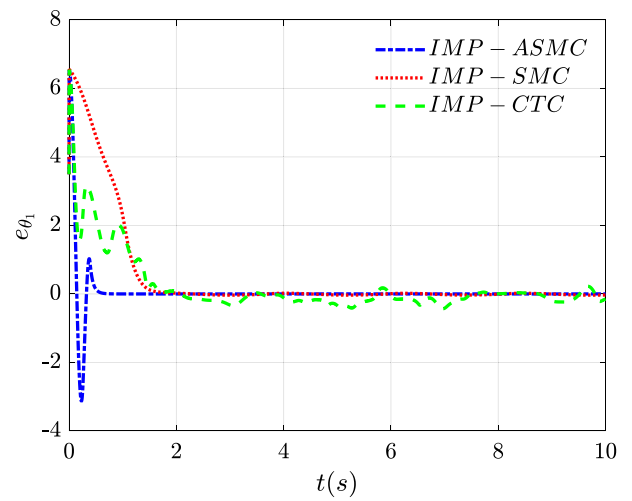$$\dot{V} \leq -\psi V + \frac{1}{2} \sum_{i=1}^{3} \gamma_i \Omega_i \qquad (23)$$

$$\dot{V} = S^T M \dot{S} + \frac{1}{2} S^T \dot{M} S + \sum_{i=1}^{3} \tilde{\Omega}_i \dot{\hat{\Omega}}_i = S^T(\tau - CS + \Xi) + \frac{1}{2} S^T \dot{M} S + \sum_{i=1}^{3} \tilde{\Omega}_i \dot{\hat{\Omega}}_i$$

$$= S^T \left(-\left[\Gamma S + \Lambda \text{sgn}(S)\right] + \Xi\right) + \frac{1}{2} S^T (\dot{M} - 2C) S + \sum_{i=1}^{3} \tilde{\Omega}_i \dot{\hat{\Omega}}_i \qquad (19)$$

$$\leq -S^T \Lambda S - \sum_{i=1}^{3} \tilde{\Omega}_i \left[\|\vartheta\| . \|\Phi\|^{i-1} - \gamma_i \hat{\Omega}_i\right]$$

The following equality can be useful to simplify the above inequality.

$$\tilde{\Omega}_i \dot{\hat{\Omega}}_i = \|S\| \tilde{\Omega}_i \|\Phi\|^i + \gamma_i \hat{\Omega}_i \Omega_i - \gamma_i \hat{\Omega}_i^2 \qquad (20)$$

Where $\psi = \min_i \left\{\lambda(\Lambda)_{i_{\min}}, \max\left\{\overline{m}/2, 1/2\right\}\right\}$. By using $0 < \psi < \kappa$, yields:

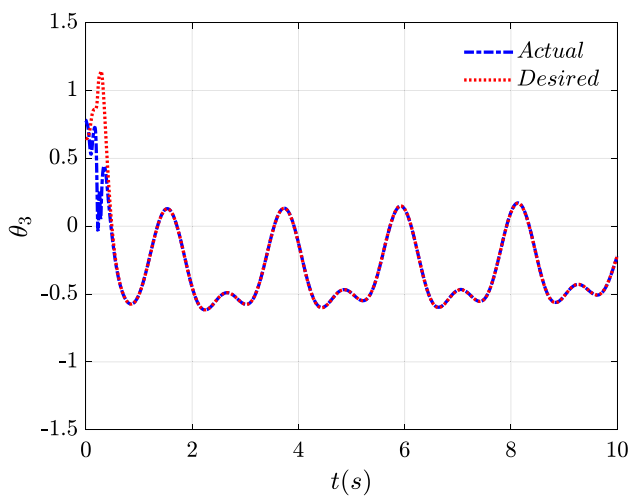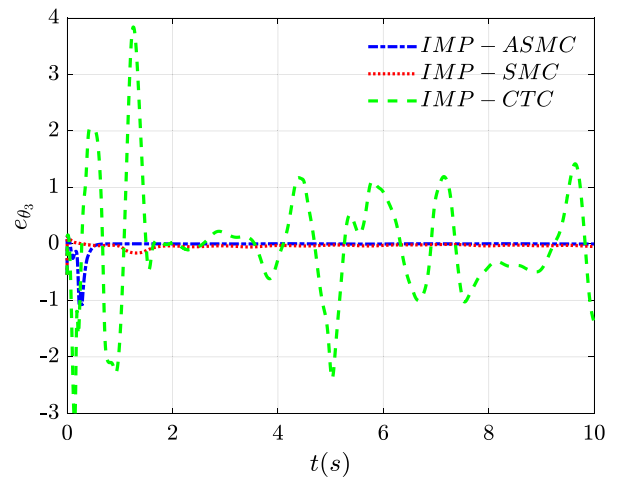**Fig. 2** Schematic of proposed IMP-ASMC control block diagram
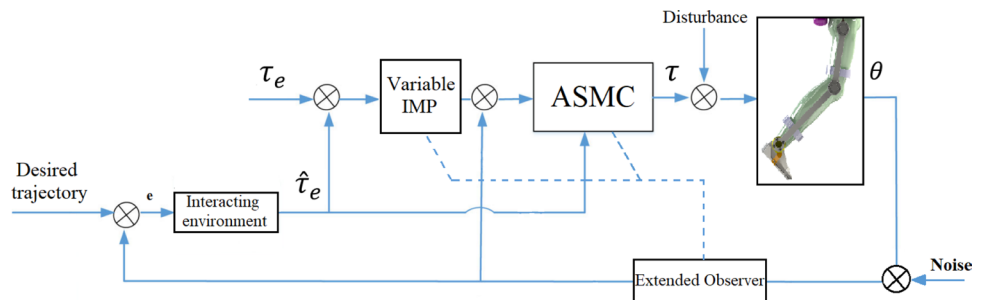
(a_1)

(b_1)
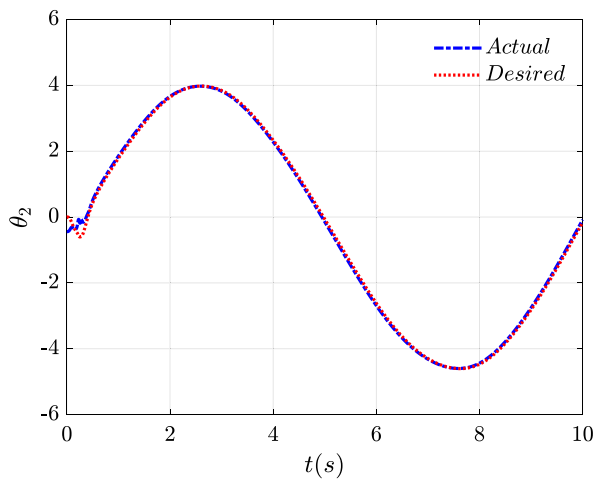
(a_2)
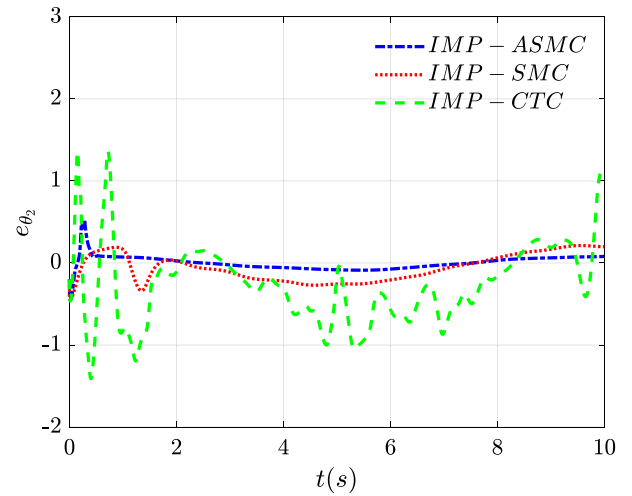
(b_2)

(a_3)

(b_3)

◄**Fig. 3** Tracking performance of proposed IMP-ASMC controller. **a** Subfigures (a_1), (a_2), and (a_3) compare the actual (blue) and desired (red) trajectories for joints θ_1, θ_2, and θ_3, respectively. **b** Subfigures (b_1), (b_2), and (b_3) present depict the corresponding joint tracking errors and provide a comparison with different controllers

$$\dot{V} \leq -\kappa V - (\psi - \kappa)V + \frac{1}{2}\sum_{i=1}^{3}\gamma_i\Omega_i^2 \tag{24}$$

By defining $P_B = \frac{\sum_{i=1}^{3}\gamma_i\Omega_i^2}{2(\psi-\kappa)}$, then $V \leq \max\{V(0), P\}, \forall t \geq 0$, it can be perceived that $\dot{V} \leq -\kappa V$, which ensures finite-time convergence of the Lyapunov function inside the ball defined by P_B.

Remark 1: The definition of the expressed Lyapunov function in Eq. (22) gives $V = \frac{1}{2}|S|^2$. Consequently, we have the ultimate bound ω which is global and uniform as it is free from initial condition. This completes the proof.

2.2 Finite-time convergence

In this section, finite-time stability of the sliding surface is investigated. When the closed-loop system reaches the sliding surface, $S = 0$, then

$$\dot{e} + \int_0^t \left(\lambda_1\|e\|^p\frac{e}{\|e\|} + \lambda_2\|\dot{e}\|^q\frac{\dot{e}}{\|\dot{e}\|}\right)d\tau = 0 \tag{25}$$

Taking time derivative of Eq. (23), yields:

$$\ddot{e} + \lambda_1\|e\|^p\frac{e}{\|e\|} + \lambda_2\|\dot{e}\|^q\frac{\dot{e}}{\|\dot{e}\|} = 0 \tag{26}$$

By defining $z_1 = e$ and $z_2 = \dot{e}$, Eq. (24) is rewritten as:

$$\dot{z}_1 = z_2 \tag{27}$$

$$\dot{z}_2 = -\lambda_1\frac{z_1}{z_1^{1-q}} - \lambda_2\frac{z_2}{z_2^{1-p}} \tag{28}$$

Now, the Lyapunov function is defined as:

$$V_1 = \frac{\lambda_1\|z_1\|^{q+1}}{q+1} + \frac{\|z_2\|^2}{2} \tag{29}$$

By taking the time derivative of Eq. (27), we obtain:

$$\begin{aligned}\dot{V}_1 &= \lambda_1\|z_1\|^{q-1}z_1^T.z_1 - z_2^T\left(\lambda_1\frac{z_1}{\|z_1\|^{1-q}} + \lambda_2\frac{z_2}{\|z_2\|^{1-p}}\right) \\ &= \lambda_1\|z_1\|^{q-1}z_1^T.z_1 - \lambda_1\|z_1\|^{q-1}z_2^Tz_1 - \lambda_2\|z_2\|^{p-1}z_2^Tz_2 = -\lambda_2\|z_2\|^{p+1}\end{aligned} \tag{30}$$

By applying LaSalle's invariance principle, the asymptotic convergence of z_1 and z_2 to zero is guaranteed. Thus,

the tracking error can be driven to the origin along $S = 0$ in a finite time. This completes the proof.

2.3 Variable impedance strategy

Controlling the applied force of the robot to the human is the most important challenge of rehabilitation robots. Various strategies have been proposed for such force control [44–46]. The fundamental principle of impedance control is to provide assistance through rehabilitation robots only when necessary. In essence, the robot offers greater support to patients with significant disabilities, while providing lesser assistance to those with minor disabilities. The aim is to customize the level of support according to the individual needs of each patient, ensuring that the robot avoids unnecessary intervention when the patient is capable of independently performing the task. This personalized approach optimizes the effectiveness of the rehabilitation process by delivering the suitable amount of assistance at the appropriate time. The goal of the impedance in configuration space is to develop a dynamic relation between the external force and configuration error, as [40–48]:

$$M_d(\ddot{\theta} - \ddot{\theta}_d) + C_d(\dot{\theta} - \dot{\theta}_d) + K_d(\theta - \theta_d) = \tau_e \tag{31}$$

in which M_d, C_d, K_d are the desired inertia, damping and stiffness, respectively; and τ_e represents the external force or torque applied to the system. These matrices are adjusted by the user in order to determine the behavior of the soft robot against external forces. In this research, the time-varying impedance control strategy is utilized. It means a virtual mass, spring and damper is applied such that they are variable with the time and can change the impedance of the whole system appropriately. It should be noted that asymptotic stability of the system can still be guaranteed if theses matrices are varying as follows.

Theorem 2: We consider M_d, C_d, K_d as symmetric and positive definite matrices and also continuously differentiable varying profiles. It can be proved that the system of Eq. (29), when $\tau_e = 0$, is uniformly globally and asymptotically stable (UGAS) if there exist a positive constant α so that:

$$\dot{M}_d + \alpha M_d - C_d \leq 0 \tag{32}$$

$$(\alpha^2 + 2\alpha)\dot{M}_d - \alpha\ddot{M}_d + \alpha\dot{C}_d + \dot{K}_d - 2\alpha K_d \leq 0 \tag{33}$$

Proof: In order to perform the stability analysis, we use a Lyapunov function:

$$V = \frac{1}{2}(\Upsilon^T M_d \Upsilon + \Xi^T \mu \Xi) \tag{34}$$
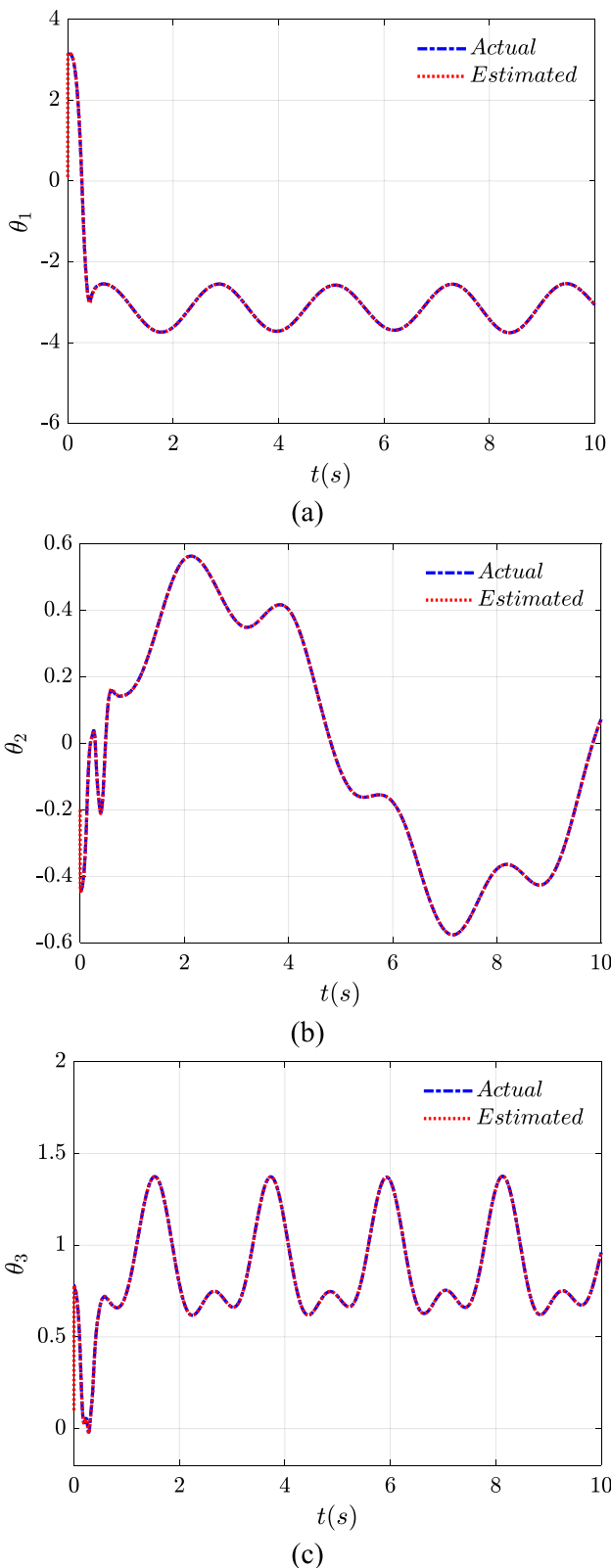
Fig. 4 The estimated states for θ_1, θ_2, and θ_3 using the proposed IMP-ASMC controller

where μ is a symmetric and positive definite matrix and $\Upsilon = \dot{\Xi} + \alpha \Xi . \Xi = \Omega - \Omega_d$. By taking the time derivative of Eq. (32), we obtain:

$$\dot{V} = \Upsilon^T M_d (\ddot{\Xi} + \alpha \dot{\Xi}) + \frac{1}{2} \Upsilon^T \dot{M}_d \Upsilon + \Xi^T \mu \dot{\Xi} + \frac{1}{2} \Xi^T \dot{\mu} \Xi \quad (35)$$

When $\tau_e = 0$,

$$\dot{V} = \dot{\Xi}^T (\dot{M}_d + \alpha M_d - C_d) \dot{\Xi} + \dot{\Xi}^T (\alpha^2 M_d + \alpha \dot{M}_d - \alpha C_d - K_d + \mu) \Xi$$
$$+ \Xi^T \left(\alpha^2 \dot{M}_d + \alpha^2 M_d + \frac{1}{2} \dot{\mu} - \alpha K_d \right) \Xi \quad (36)$$

By defining $\mu = -\alpha^2 M_d - \alpha \dot{M}_d + K_d + \alpha C_d$ and $\dot{\mu} = -\alpha^2 \dot{M}_d - \alpha \ddot{M}_d + \dot{K}_d + \alpha \dot{C}_d$, then:

$$\dot{V} = \dot{\Xi}^T (\dot{M}_d + \alpha M_d - C_d) \dot{\Xi} + \Xi^T \left[\left(\frac{\alpha^2}{2} + \alpha \right) \dot{M}_d \right.$$
$$\left. - \frac{\alpha}{2} \ddot{M}_d + \frac{\alpha}{2} \dot{C}_d + \frac{\dot{K}_d}{2} - \alpha K_d \right] \Xi \quad (37)$$

In order to stabilize the system, the following inequality must be hold:

$$\dot{M}_d + \alpha M_d - C_d \leq 0 \quad (38)$$

$$(\alpha^2 + 2\alpha) \dot{M}_d - \alpha \ddot{M}_d + \alpha \dot{C}_d + \dot{K}_d - 2\alpha K_d \leq 0 \quad (39)$$

Which completes the proof.

The conditions defined in Eq. (36) and Eq. (37) impose constraints on the impedance matrices that can be determined using an optimization procedure. In order to satisfy the necessary conditions for Theorem 2 and also least conservative constraints, α should be determined using:

$$\alpha = \min \left(\frac{\lambda_{\min}(C_d) + \lambda_{\max}(\dot{M}_d)}{\lambda_{\max}(M_d)} \right) \quad (40)$$
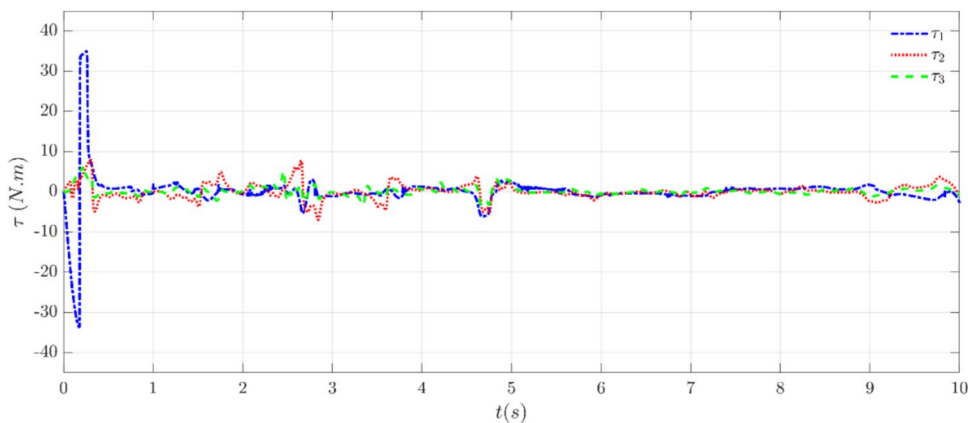
To demonstrate the systematic procedure, let us define a symmetric and negative definite matrix as $B = \dot{M}_d + \alpha M_d - C_d$ whose terms comprise symmetric matrices. For negativity of this matrix, its maximum eigenvalue $\lambda_{\max}$ must be negative. Based on the triangle inequality for supremum norm, we have:

$$\lambda_{\max}(B) = \sup v^T B v \leq \sup v^T \dot{M}_d v$$
$$+ \sup v^T (\alpha M_d) v \sup v^T (-C_d) v . \lambda_{\max}(B)$$
$$\leq \lambda_{\max}(\dot{M}_d) + \lambda_{\max}(\alpha M_d) - \lambda_{\min}(C_d) \quad (41)$$

and for satisfying the negative definiteness of B, $\lambda_{\max}(\dot{M}_d) \leq \lambda_{\min}(C_d) - \lambda_{\max}(\alpha M_d)$. We move to the second constraint that imposes a limitation on the variation of stiffness matrix. Let us consider $Q = (\alpha^2 + 2\alpha) \dot{M}_d - \alpha \ddot{M}_d + \alpha \dot{C}_d + \dot{K}_d - 2\alpha K_d$ and similar to the first constraint using the triangle inequality, then:

Fig. 5 The control effort or joint torques exerted by the proposed controller on the three joint (τ_1, τ_2, τ_3 indicate the torques related to θ_1, θ_2, and θ_3, respectively)

$$\lambda_{\max}(\dot{K}_d) \le 2\alpha\lambda_{\min}(k_d) - \alpha\lambda_{\max}(C_d) - (\alpha^2 + 2\alpha)\lambda_{\min}(C_d)$$
$$+ \alpha^2(\alpha + 2)\lambda_{\max}(M_d) + \alpha\lambda_{\min}(\ddot{M}_d) \tag{42}$$

Hence, the validity of the impedance profiles can be guaranteed through these conditions, which completes the proof of the stability of varying impedance control without dependency on state measurements.

2.4 Extended state observer

Since direct measuring of the forces and states are quiet challenging for a rehabilitation robot (specifically in view of practical application), an extended state observer is designed to measure the output signals (states variables). So, the dynamic model can be rewritten as:

$$\ddot{\theta} = \psi + M^{-1}\tau \tag{43}$$

$$\psi = -M^{-1}\big(C\dot{\theta} + G + \tau_d\big) \tag{44}$$

If $z_1 = \theta$ and $z_2 = \dot{\theta}$ and state variable $z_3 = \psi$, the mathematical model of the high-order observer is expressed as follows:

$$\dot{z}_1 = z_2 \tag{45}$$

$$\dot{z}_2 = z_3 + b_0\tau \tag{46}$$

$$\dot{z}_3 = \dot{\psi} \tag{47}$$

With the definition $\tilde{z} = z_1 - \hat{z}_1$, the nonlinear observer is introduced as follows:

$$\dot{\hat{z}}_1 = \hat{z}_2 + k_{01}\tilde{z}_1 \tag{48}$$

$$\dot{\hat{z}}_2 = \hat{z}_3 + b_0\tau + k_{02}\text{fal}\big(\tilde{z}_{1,0.5}, h\big) \tag{49}$$

$$\dot{\hat{z}}_3 = k_{03}\text{fal}\big(\tilde{z}_{1,0.25}, h\big) \tag{50}$$

$$\text{fal}(X, \sigma, h) = \begin{cases} \frac{\sigma^2}{h^{1-\sigma}}X & |X| \le h \\ |X|^\sigma\text{sgn}(X)\sigma^2 & |X| > h \end{cases} \tag{51}$$

Where $\hat{z}_i$, k_{0i}, X are the estimated values of z_i, observer gain and input error of the nonlinear function, respectively. Also $0 < \sigma < 1$ is the accuracy index and h represents the width of the linear region of the nonlinear function.

The overall schematic of proposed control block diagram, called IMP-ASMC, can be seen in Fig. 2.

3 Results and discussions

To demonstrate the effectiveness of the proposed controller in tracking the desired trajectories and providing appropriate interaction with the user, some sort of simulations is conducted. It is worth to note that the key physical parameters of a typical adult that used for all the simulations are shown in Table 1. Since the extracted dynamic model contains uncertainties, the developed approach is implemented on a virtual model derived with the assistance of MATLAB SimScape. Furthermore, in order to show the robustness of the proposed controller, parametric uncertainties and time-varying disturbances are applied in all simulations. The uncertainties were introduced by modifying each constant parameter of the model by approximately 20% to assess the response of the system. This adjustment accounts for variations in physical parameters such as mass or link lengths, simulating real-world conditions where exact values may not be known.
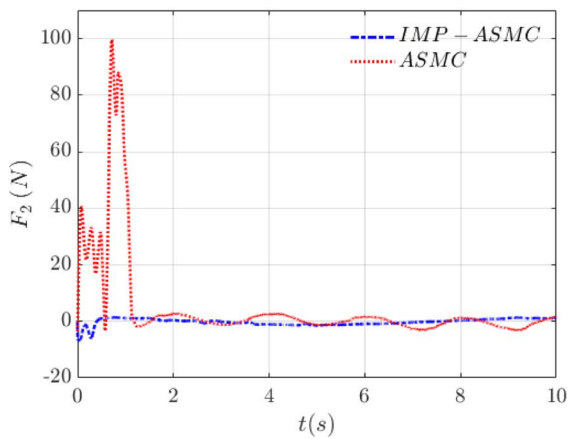
Figure 3 illustrates the tracking performance of the proposed controller, i.e., IMP-ASMC, for a natural walking trajectory from [30, 49]. Subfigures (a_1), (a_2) and (a_3) compare the actual (blue) and desired (red) trajectories for the joints θ_1, θ_2, and θ_3, respectively. Further, subfigures
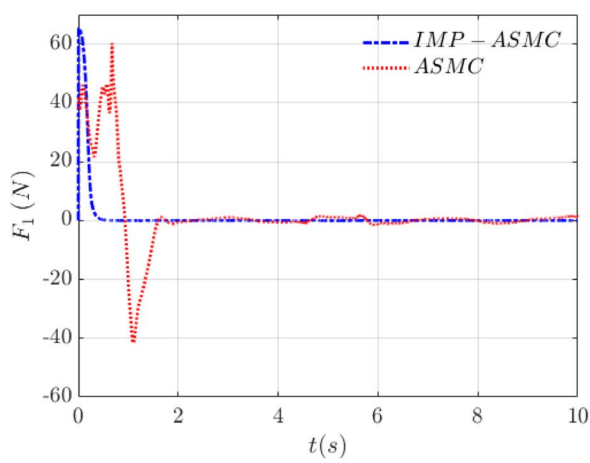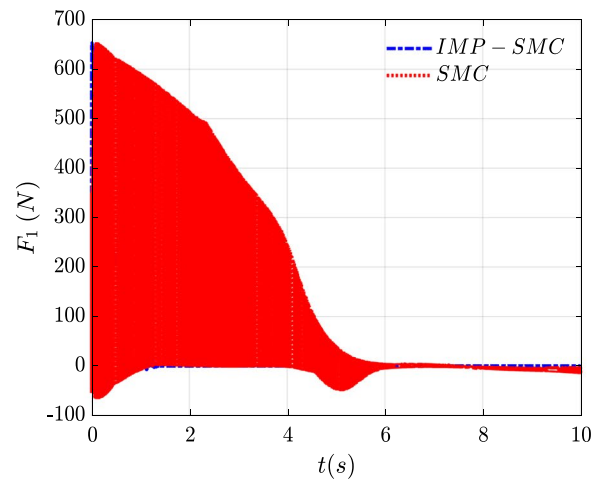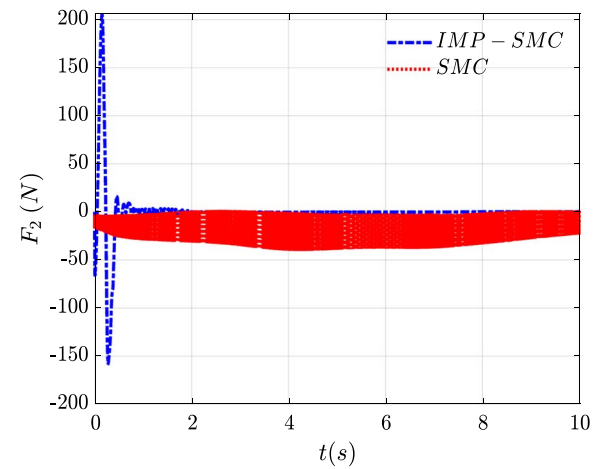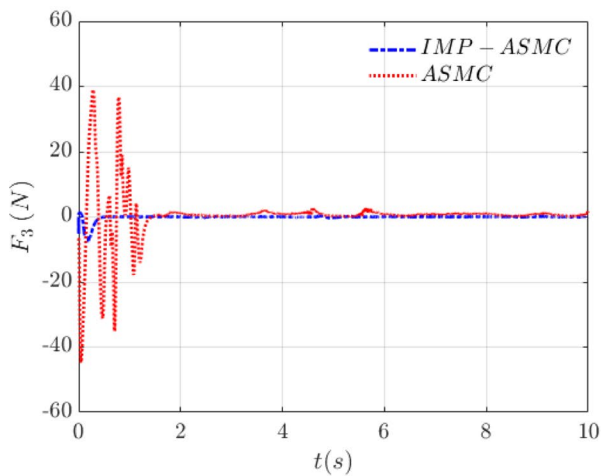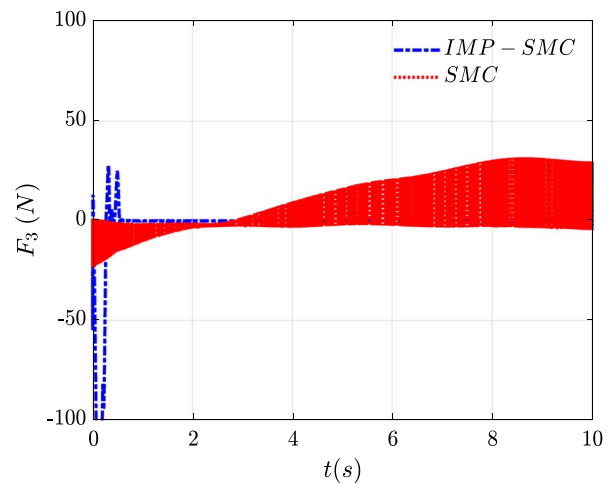
(a_1) (b_1)

(a_2) (b_2)

(a_3) (b_3)

Fig. 6 Interaction forces between the robot and the patient **a** Subfigures (a_1), (a_2), and (a_3) compare the interaction forces at joints θ_1, θ_2 and θ_3, respectively, for the proposed IMP-ASMC controller (blue) and the pure ASMC controller (red). **b** Subfigures (b_1), (b_2), and (b_3) compare the interaction forces at joints θ_1, θ_2, and θ_3; for the basic IMP-SMC (blue) and pure SMC (red) controllers

Table 2 A comparative analysis presents the average error of the obtained data relative to similar work

		IMP-ASMC	IMP-SMC	IMP-CTC	ASTSM [30, 31]
Hip angle error e_{θ_1}	Average	0.005	0.136	0.356	not discussed
Hip angle error e_{θ_2}	Average	0.009	0.153	0.381	0.194
Knee angle error e_{θ_3}	Average	0.004	0.009	0.444	0.166
Control effort u_1	Average	1.85	–	–	not discussed
Control effort u_2	Average	1.221	–	–	$2 \leq torque \leq 5$
Control effort u_3	Average	0.514	–	–	$2 \leq torque \leq 5$
Interaction force F_1	Average	0.09	2.127	–	not discussed
Interaction force F_2	Average	0.06	1.547	–	Almost 0.1
Interaction force F_3	Average	0.03	0.571	–	Almost 0.1

(b_1), (b_2), and (b_3) depict the corresponding joint tracking errors and provide a comparison with different well-known impedance-based controllers, i.e., the sliding mode controller, IMP-SMC, and the computed torque controller, IMP-CTC. Each control scheme was tuned to optimize its performance within the given uncertainties, allowing for a comprehensive comparison of their capabilities in handling uncertain dynamics. It can be clearly seen that the proposed controller maintains the tracking accuracy in an acceptable range under the detrimental effects of exogenous disturbance, uncertainty and interaction with the environment. The fluctuation of joint angles in the beginning period comes from the change in the desired trajectory imposed by the impedance control strategy. The remaining interval provides a general overview of the smooth tracked trajectory. Also, for the sake of comparison, it can be clearly seen that the proposed controller outperforms than IMP-SMC and IMP-CTC schemes. Besides, since IMP-ASMC and IMP-SMC strategies are robust against adversaries such as uncertainty and interaction with the environment, they provide more efficient performance than IMP-CTC. In general, the associated IMP-CTC controller caters poorest performance due to showing the largest tracking errors. This indicates the superiority of the proposed adaptive impedance controller rather than others.

The estimated states by the proposed observer are also depicted in Fig. 4, illustrating the accuracy and robustness of the observer in estimating the required signals for instance. Indeed, the convergence time in the beginning of the interval shows the effectiveness and superiority of the observer while the estimated signal is started from a different point of the main signal.

Figure 5 illustrates the control efforts or joint torques exerted by the proposed controller on the three joints, namely τ_1, τ_2 and τ_3. It is observed that the maximum torques remain within the saturation limit defined for the actuators. It is crucial to avoid excessive control effort as it can lead to discomfort for the patient and potentially disrupt their natural and physiological movements.

The reduction of interactive forces in rehabilitation robots is a crucial objective. Figure 6 (a_1), (a_2), and (a_3) illustrates the interaction forces induced between the robot and the patient at joints θ_1, θ_2 and θ_3, respectively, using the proposed IMP-ASMC controller. A comparison is made with the corresponding interaction forces generated by a pure ASMC controller, which does not employ an impedance strategy. The results clearly demonstrate that the developed control framework significantly reduces the interaction forces, whereas the pure ASMC controller generates high interaction forces that can adversely affect the performance of the control system and the comfort of the patient.

For comparison purposes, the evaluation of interaction forces was also conducted within the framework of basic sliding mode controllers. Therefore, similarly, Fig. 6 (b_1), (b_2), and (b_3) displays the interaction forces at joints θ_1, θ_2 and θ_3, for both the conventional non-impedance-based and impedance-based schemes of the basic sliding mode controller, i.e., SMC and IMP-SMC, respectively. It is important to note that CTC-type controllers have been excluded from consideration due to their consistently poor performance in this context. Upon examination, it is evident that the pure SMC controller exhibits excessive chattering phenomena and fluctuations in the interaction forces, which can compromise the motion stability and patient comfort in the rehabilitation robot. IMP-SMC, on the other hand, eliminates the chattering phenomenon but exhibits large peaks in the interaction forces at the beginning.

Table 2 provides a summary of the comparison of tracking performance among three "variable impedance" controllers: the proposed one, IMP-ASMC, along with IMP-SMC and IMP-CTC, as well as a "fixed impedance" adaptive sliding mode controller known as ASTSM, recently discussed in [30, 31].
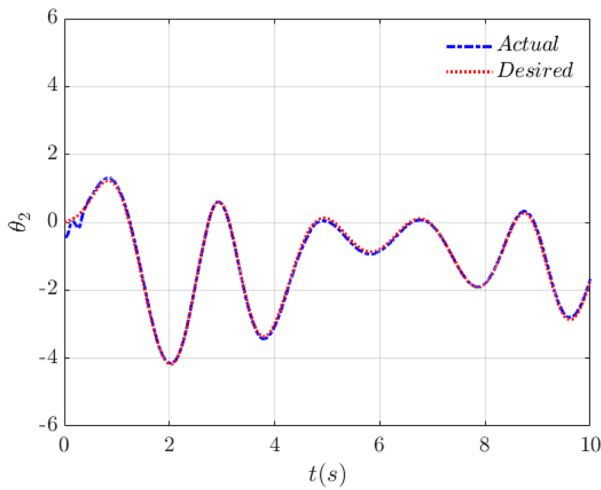
To illustrate the capability of the proposed controller, an alternative trajectory tracking is also investigated and briefly shown in Fig. 7, following the same format of Fig. 3. It is still evident that the proposed controller outperforms the IMP-SMC and IMP-CTC schemes. Additionally, the IMP-ASMC and IMP-SMC strategies exhibit robustness against
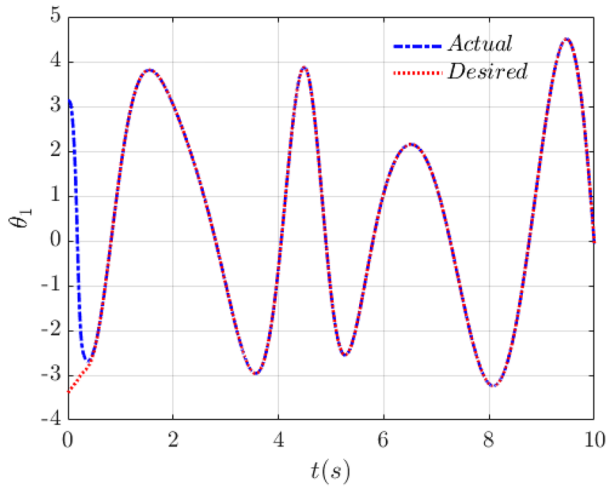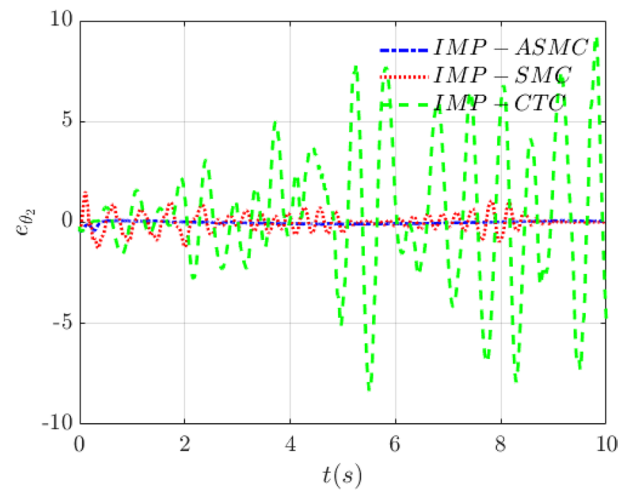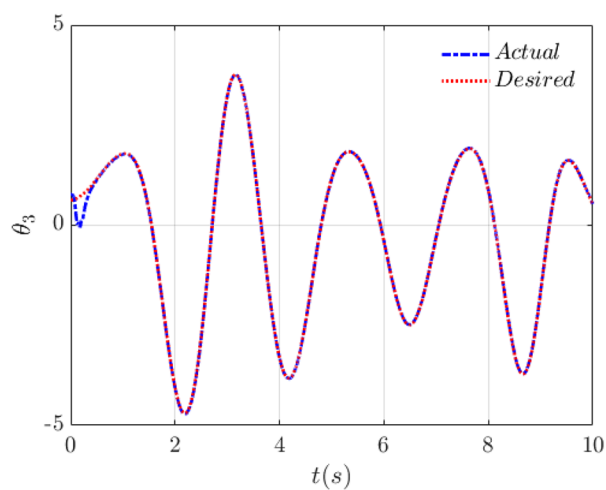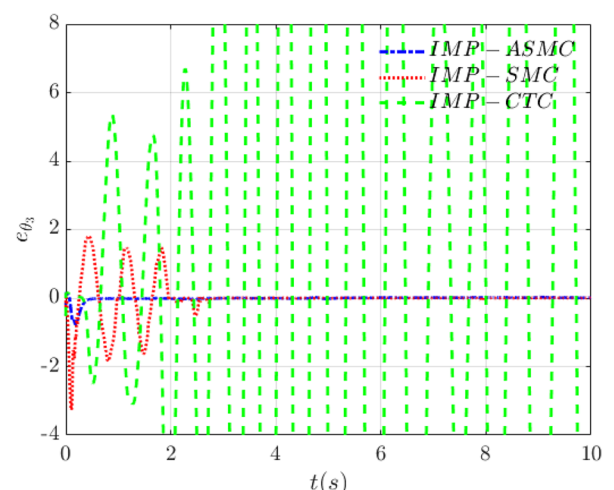
(a_1)
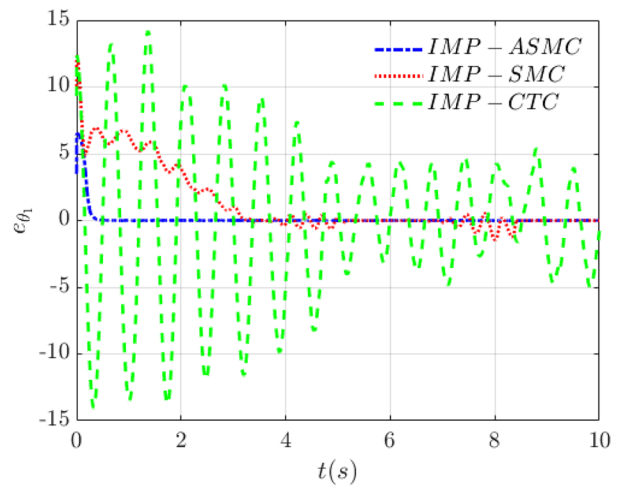
(b_1)

(a_2)

(b_2)

(a_3)

(b_3)

◀**Fig.7** Tracking performance of IMP-ASMC controller for the second mentioned trajectory. **a** Comparison of actual versus desired joint trajectories θ_1, θ_2, and θ_3 in subfigures ($\mathbf{a_1}$), ($\mathbf{a_2}$), and ($\mathbf{a_3}$). **b** The corresponding joint tracking errors and comparison with different controllers in subfigures ($\mathbf{b_1}$), ($\mathbf{b_2}$), and ($\mathbf{b_3}$)

uncertainties and environmental interactions, resulting in more efficient performance compared to the IMP-CTC scheme.

Overall, the findings indicate that the proposed controller excels in performance by consistently achieving the lowest average errors even in the presence of bounded uncertainties. Furthermore, it demonstrates superior capabilities in minimizing interaction forces and control effort, particularly when encountering variable impedance. These results confirm that the IMP-ASMC controller not only provides satisfactory performance but also effectively reduces chattering and undesirable forces, underscoring its effectiveness in the specific context under study.

Actually, in the field of robotic rehabilitation for physically disabled patients, the interface between the rehabilitation robot and the patient is crucial. Disabled patients may be hesitant to engage with a physiotherapist, let alone a rehabilitation robot. Indeed, in the realm of rehabilitation robotics, an advanced controller like the one proposed can equip robots with the following necessary capabilities to address rehabilitation issues effectively:

- Tracking the optimal walking path determined by the physiotherapist, even in the presence of uncertainties, which significantly facilitate the proper rehabilitation process.
- Ensuring the patient's comfort within the device and avoiding the application of undesirable and chattering forces on the patient to enhance ease of use.
- Providing tailored assistance to meet the patient's specific needs. Detecting the appropriate level of support directly impacts the reduction of contact forces between the patient and the robot, aligning with the core principle of the impedance control strategy, where minimizing contact forces during treatment is crucial. Additionally, the proposed impedance strategy is adaptable to accommodate communication with disabled patients exhibiting unknown and unpredictable movements.
- Minimizing control effort is also critical. By reducing the control effort in the robot's joints, we can ensure the application of sufficient force to the patient in the safest possible positions

4 Conclusion

In this study, we have proposed a novel control strategy for a lower-limb gait rehabilitation exoskeleton, named IMP-ASMC. This approach integrates a model-free adaptive sliding mode control, which ensures the sliding condition to mitigate the effects of unknown uncertainties and prevents the overestimation of the control gain in the presence of uncertainty. Additionally, the strategy incorporates a variable impedance approach that enables the system's impedance to adapt dynamically over the gait, maintaining accurate tracking of desired joint trajectories. The stability of the proposed control strategy is rigorously proven using Lyapunov theory, providing confidence in its effectiveness. One important advantage of the proposed approach is its model-free nature, making it efficient for real-time applications.

The effectiveness of the proposed control strategy was thoroughly evaluated through simulations on a dynamic model, and comparative evaluations were conducted against two nonlinear controllers: conventional sliding mode control (SMC) and computed torque controller (CTC). The results confirm the assumptions of the proposed control approach, achieving a balance between force reduction and accurate gait trajectory tracking. It was shown that the incorporation of variable impedance in the control strategy significantly reduces the interaction forces experienced by both the robot and the user. Furthermore, the proposed controller demonstrates higher robustness compared to the other controllers when faced with increased uncertainties and external forces, outperforming them in challenging operating conditions.

Our findings contribute to the advancement of exoskeleton robotics by providing a foundation for reducing interaction forces between the patient and the robot, particularly in the field of rehabilitation where ensuring user comfort and safety is paramount. The presented control strategy has the potential to enhance the performance and usability of lower-limb exoskeleton robots, ultimately benefiting individuals undergoing rehabilitation. In the future work, we intend to investigate the findings of the variable impedance control along with the proposed controller, on an actual rehabilitation robot.

References

1. Barbosa AM, Carvalho JCM, Gonçalves RS (2018) Cable-driven lower limb rehabilitation robot. J Braz Soc Mech Sci Eng 40:1678–5878
2. Diaz I, Gil JJ, Sanchez E (2011) Lower-limb robotic rehabilitation: literature review and challenges. J Robot Article ID 759764:11
3. Rodrigues LAO, Gonçalves RS (2020) Development of a Parallel robotic body weight support for human gait rehabilitation. In: Bastos-Filho TF, Mariade Oliveira Caldeira, Frizera-Neto EA

(eds) In Brazilian Congress on biomedical engineering. Springer International Publishing, Cham, pp 593–598

4. Pohl M, Werner C, Holzgraefe M, Kroczek G, Wingendorf I, Hoölig G, Koch R, Hesse S (2007) Repetitive locomotor training and physiotherapy improve walking and basic activities of daily living after stroke: a single-blind, randomized multicentre trial (DEutsche GAngtrainerStudie, DEGAS). Clin Rehabil 21(1):17–27

5. Martins M M, Frizera Neto A, Santos C and Ceres R, (2011) "Review and classification of human gait training and rehabilitation devices," Proceedings of the 11th European Association for the Advancement of Assistive Technology in Europe (AAATE'11), Maastricht, Netherlands

6. Baser O, Kizilhan H, Kilic E (2019) Biomimetic compliant lower limb exoskeleton (BioComEx) and its experimental evaluation. J Braz Soc Mech Sci Eng 41:1678–5878

7. Bogue R (2009) Exoskeletons and robotic prosthetics: a review of recent developments. Ind Robot Int J 36:421–427

8. Colombo G, Joerg M, Schreier R, Dietz V (2007) Treadmill training of paraplegic patients using a robotic orthosis. J Rehabil. Res. Dev 37:693–700

9. Marchal-Crespo Laura, Riener Robert (2022) Technology of the robotic gait orthosis lokomat. In: Reinkensmeyer DJ, Marchal-Crespo L, Dietz V (eds) Neurorehabilitation Technology. Springer International Publishing, Cham, pp 665–681

10. Kyaw PK, Sandar K, Khalid M, Juan W, Li Y, Chen Z (2013) Opportunities in robotic exoskeletons hybrid assistive limb SUIT (MT5009). Robot Exos Becom Econ Feasible 21:1

11. Oyman EL, Korkut M Y, Yilmaz C, Bayraktaroglu ZY, Selcuk Arslan M (2022) Design and control of a cable-driven rehabilitation robot for upper and lower limbs. Robotica 40:1–37

12. Reinoso MJ, Minchala LI, Ortiz P, Astudillo DF, Verdugo D (2016) Trajectory tracking of a quadrotor using sliding mode control. IEEE Lat Am Trans 14:2157–2166

13. Wu X, Xiao B, Qu Y (2019) Modeling and sliding mode-based attitude tracking control of a quadrotor UAV with time-varying mass. ISA Trans 124:443

14. Utkin VI, Poznyak AS (2013) Adaptive sliding mode control with application to super-twist algorithm: equivalent control method. Automatica 49:39–47

15. Zhihong M, Paplinski AP, Wu HR (1994) A robust MIMO terminal sliding mode control scheme for rigid robotic manipulators. IEEE Trans Autom Control 39(12):2464–2469

16. Yu X, Zhihong M (2002) Fast terminal sliding-mode control design for nonlinear dynamical systems. IEEE Trans Circuit Syst Fundament Theory Appl 49(2):261–264

17. Feng Y, Yu X, Man Z (2002) Non-singular terminal sliding mode control of rigid manipulators. Automatica 38(12):2159–2167

18. Yang L, Yang J (2011) Nonsingular fast terminal sliding-mode control for nonlinear dynamical systems. Int J Robust Nonlinear Control 21(16):1865–1879

19. Thanh HLNN, Hong SK (2018) Quadcopter robust adaptive second order sliding mode control based on PID sliding surface. IEEE Access 6:66850–66860

20. Derafa L, Benallegue A, Fridman L (2012) Super twisting control algorithm for the attitude tracking of a four rotors UAV. J Franklin Inst 349(2):685–699

21. Mokhtari M, Taghizadeh M, Ghaf-Ghanbari P (2022) Adaptive second-order sliding model-based fault-tolerant control of a lower-limb exoskeleton subject to tracking the desired trajectories augmented by CPG algorithm. J Braz Soc Mech Sci Eng 44:1678–5878

22. Liao Y, Du T, Jiang Q (2019) Model-free adaptive control method with variable forgetting factor for unmanned surface vehicle control. Appl Ocean Res 93:101945

23. Qin H, Chen H, Sun Y (2020) Distributed finite-time fault-tolerant error constraint containment algorithm for multiple ocean bottom flying nodes with tan-type barrier Lyapunov function. Int J Robust Nonlinear Control 30(13):5157–5180

24. Salter RB (1993) "Intra-articular fractures," Continuous Passive Motion (CPM). Williams & Wilkins, Baltimore, pp 79–93

25. Hogan N (1985) Impedance control: an approach to manipulation: parts I-III. J Dyn Syst Meas Contr 107:1–24

26. N. Hogan (1984) "Impedance Control: An Approach to Manipulation," paper read at the American Control Conference, San Diego

27. Shota M, Kousei N, Nobutomo M, Shigeyasu K (2008) Impedance control of two d.o.f CPM device for upper limb disorders. IFAC Proc Vol 41:9087–9092

28. M F Michael Bernhardt G Colombo R Riener (2005) "Hybrid force-position control yields cooperative behaviour of the rehabilitation Robot LOKOMAT," International Conference on Rehabilitation Robotics, Chicago, IL, USA

29. Riener R, Lunenburger L, Jezernik S, Anderschitz M, Colombo G, Dietz V (2005) Patient cooperative strategies for robot-aided treadmill training: first experimental results. IEEE Trans Neural Syst Rehabilitat Eng 13(3):380–394

30. Mokhtari M, Taghizadeh M, Mazare M (2021) Impedance control based on optimal adaptive high order super twisting sliding mode for a 7-DOF lower limb exoskeleton. Meccanica 56:535–548

31. Mokhtari M, Taghizadeh M, Mazare M (2020) Hybrid adaptive robust control based on CPG and ZMP for a lower limb exoskeleton. Robotica 39:181–199

32. R M Andrade S Sapienza and P Bonato (2019) "Development of a transparent operation mode for a lower-limb exoskeleton designed for children with cerebral palsy," International Conference on Rehabilitation Robotics (ICORR), Toronto, Canada, p 512–517

33. Andrade RM, Sapienza S, Fabara EE, Bonato P (2021) "Trajectory tracking impedance controller in 6-DoF lower-limb exoskeleton for over-ground walking training: preliminary results", International symposium on medical robotics (ISMR). Atlanta, USA, pp 1–6

34. Mendoza-Crespo R, Soto R, Pons JL (2017) Transparent Mode for lower limb exoskeleton. Wearable Robotics: Challenges and Trends. Springer International Publishing, Cham, pp 421–425

35. Andrade RM, Sapienza S, Mohebbi A, Fabara EE, Bonato P (2024) Overground walking with a transparent exoskeleton shows changes in spatiotemporal gait parameters. IEEE J Trans Eng Health Med 12:182–193

36. Song A, Pan L, Xu G, PLi H (2015) Adaptive motion control of arm rehabilitation robot based on impedance identification. Robot J 33:1795–1812

37. Jung S, Hsia TC, Bonitz RG (2004) Force tracking Impedance control of robot manipulators under unknown envierment. IEEE Trans Control Syst Technol 12:474–483

38. Stanisic RZ, Fernandez AV (2012) Adjusting the parameters of the mechanical impedance for velocity, impact and force control. Robot J 30:583–597

39. Huang AC, Lee KJ, Du WL (2023) Contact force cancelation in robot impedance control by target impedance modification. Robot J 41:1733–1748

40. Mazare M, Tolu S, Taghizadeh M (2022) Adaptive variable impedance control for a modular soft robot manipulator in configuration space. Meccanica 57:1–15

41. J C Chan-Yul Jung SH Park J Lee CH Kim and S Kim (2014) "Design and Control of an Exoskeleton System for Gait Rehabilitation Capable of Natural Pelvic Movement." IEEE/RSJ International Conference on Intelligent Robots and Systems

42. Al-Rahmani N, Mohan DM, Awad MI, Wasti SA, Hussain I, Khalaf K (2022) Lower-limb robotic assistance devices for drop foot a review. IEEE 10:5196–51994

43. Vukobratovic M, Borovac B, Surla D, Stokic D (1990) Biped locomotion. Springer-Verlag, Berlin

44. Bradley D, Acosta-Marquez C, Hawley M, Brown S, Brown sell S, Ender P, Mawson S (2009) Naxos–The design, development and evaluation of a rehabilitation system for the lower limbs. Mechatronics 19:247–257

45. Moughamir S, Zaytoon J, Manamanni N, Afilal L (2002) A system approach for control development of lower-limbs training machines. Control Eng Pract 10:287–299

46. Stanisic RZ, Fernandez AV (2011) Adjusting the parameters of the mechanical impedance for velocity, impact and force control. Robotica 30:583–597

47. Ba K, Ma G, Yu B, Jin Z, Huang Z, Zhang J, Kong X (2020) A Nonlinear model-based variable impedance parameters control for position-based impedance control system of hydraulic drive unit. Int J Control Autom Syst 18:1806–1817

48. Zhou B, Song F, Liu Y, Fang F, Gan Y (2023) Robust sliding mode impedance control of manipulators for complex force-controlled operations. Nonlinear Dyn 111:22267–22281

49. Farzaneh Y, Akbarzadeh A, Akbari A (2014) Online bio-inspired trajectory generation of seven-link biped robot based on T–S fuzzy system. Appl Soft Comput 14:167–180